Tests to Structural Collapse of Single Degree of Freedom Frames Subjected to Earthquake Excitations

Darren Vian, M.ASCE,[1] and Michel Bruneau, M.ASCE[2]

Abstract: This paper presents and analyzes experimental results of tests of 15 four-column frame specimens subjected to progressively increasing unidirectional ground shaking to collapse. The specimens were subdivided into groups of three different column slenderness ratios: 100, 150, and 200. Within each group, the column dimensions and supported mass varied. Ground motion of varying magnitudes was required to collapse the structure tested. The experimental setup is briefly described and results are presented. Test structure performance is compared with proposed limits for minimizing $P-\Delta$ effects in highway bridge piers. The stability factor is found to have a strong relation to the relative structural performance in this regard. Performance is also compared with capacity predicted by currently used strength and stability axial-moment interaction design equations by expressing these capacities in terms of acceleration and maximum base shear (as a fraction of the system's weight). The experimental results exceeded the maximum spectral accelerations calculated when considering second-order effects, but did not when considering only member strength. Finally, an example of how to use the experimental data for analytical model verification is presented, illustrating the shortcomings/inaccuracies of using a particular simplified model with constant structural damping.

DOI: 10.1061/(ASCE)0733-9445(2003)129:12(1676)

CE Database subject headings: Collapse; Earthquakes; Building frames; Damping.

Introduction

The arbitrary lateral drift limits prescribed by earthquake-resistant design codes to prevent excessive nonstructural damage during earthquakes also indirectly ensure that structural performance is minimally affected by the effect of gravity on the lateral force resistance of structures (aka $P-\Delta$ effect). However, from the perspective of performance-based design, there is a desire to eliminate these drift limits so protection against nonlinear structural instability will therefore have to be provided by other performance-based controls. In fact, this has already occurred in some proposed bridge design specifications. As such, accurate quantification of the destabilizing effect of gravity will become essential in structures that rely on inelastic behavior to dissipate seismic input energy. Toward that end, research is needed to enhance our understanding of the conditions that ultimately lead to collapse.

Analytical models and algorithms able to reliably capture the inelastic cyclic collapse limit state as a result of earthquake excitations will need to be developed, calibrated, and validated using experimental data. To provide some of that experimental data, 15 specimens, each having four columns and designed to have a rigid beam and thus behave as single-degree-of-freedom (SDOF) systems horizontally, were subjected to shake table testing to collapse. All tests were thoroughly documented (geometry, material properties, initial imperfections, detailed results, etc.) to make results usable as benchmarks to which analytical models can be compared.

This paper presents relevant $P-\Delta$ concepts, specimen fabrication, and documentation of their pretest condition, important aspects of the experimental setup, dynamic properties measured from free vibration tests, and selected shake table test results.

Although the first and foremost objective of this project was to provide well-documented data (freely available on the web to be used by others) of tests to collapse, this paper includes results from a preliminary investigation of behavioral trends observed from the shake table results. In particular, peak responses are compared with limits proposed by others to minimize $P-\Delta$ effects in bridge piers. Specimen behavior is also investigated with respect to axial-moment strength and stability interaction limits. Finally, to illustrate how the generated experimental data could be used to develop or calibrate analytical models of inelastic behavior to collapse, experimental results are compared with those obtained using a simple analytical model. Progressive bilinear dynamic analyses are performed in two different ways and are compared with the shake table test results.

$P-\Delta$ Concepts

Fundamental Parameters

The concept of $P-\Delta$ effects under static loading can be illustrated using the SDOF structure shown in Fig. 1. In Fig. 1, $2P$ represents the force due to gravity acting on the mass lumped at the top of the structure, L is the column height, $2V$ is the lateral

[1]PhD Candidate, Dept. of Civil, Structural and Environmental Engineering, Univ. at Buffalo, Amherst, NY 14260. E-mail: vian@eng.buffalo.edu

[2]Deputy Director, MCEER, Professor, Dept. of Civil, Structural and Environmental Engineering, Univ. at Buffalo, Amherst, NY 14260. E-mail: bruneau@mceermail.buffalo.edu

Note. Associate Editor: Sashi K. Kunnath. Discussion open until May 1, 2004. Separate discussions must be submitted for individual papers. To extend the closing date by one month, a written request must be filed with the ASCE Managing Editor. The manuscript for this paper was submitted for review and possible publication on October 18, 2001; approved on February 24, 2003. This paper is part of the ***Journal of Structural Engineering***, Vol. 129, No. 12, December 1, 2003. ©ASCE, ISSN 0733-9445/2003/12-1676–1685/$18.00.

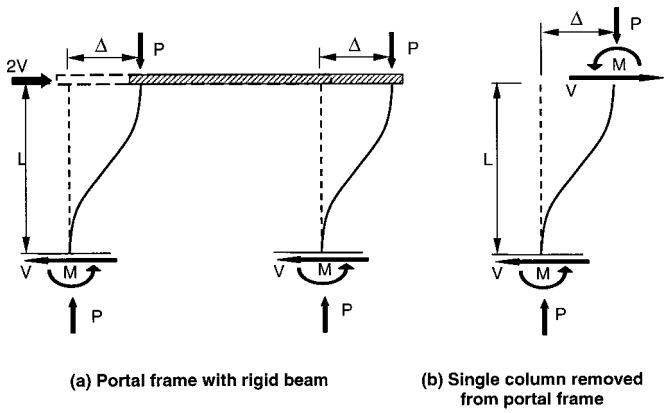

Fig. 1. Free body diagrams of typical SDOF structure: (a) portal frame with rigid beam; (b) single column removed from portal frame

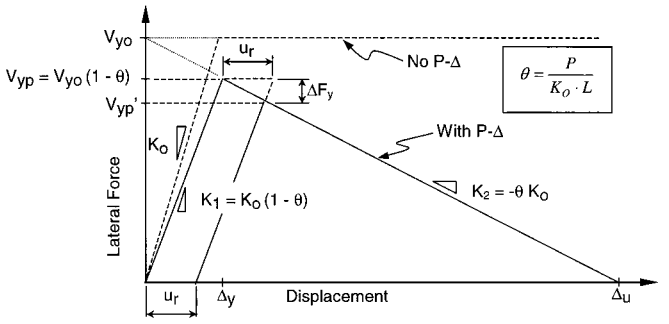

Fig. 2. Bilinear lateral force versus displacement model for SDOF structure

force on the mass, and Δ is the horizontal displacement of the mass. As the structure sways by Δ under the effect of lateral force, the product of $P\times\Delta$ produces an additional moment at the base of each column, which can be obtained by considering static equilibrium in the deformed configuration.

If the typical SDOF structure considered in Fig. 1(a) is a single-bay portal frame with an infinitely rigid beam, the elastic lateral stiffness of each column within the frame, ignoring the $P-\Delta$ effect, is given by

$$K_0=12EI/L^3 \tag{1}$$

where E = elastic modulus of the material; I = moment of inertia of the column section; and L = height of the column.

For the bilinear elastically perfect plastic model shown in Fig. 2, the ultimate lateral force, ignoring the $P-\Delta$ effect, which can be applied to each identical column of that frame, is reached when the plastic moment of the column, M_p, develops at the top and bottom of the column, and is given by

$$V_{y0}=2M_p/L \tag{2}$$

The corresponding yield displacement is

$$\Delta_y=V_{y0}/K_0 \tag{3}$$

Now, as shown in Fig. 1(b), considering $P-\Delta$ effects for a single column in the same frame, moment equilibrium gives

$$2M=VL+P\Delta \tag{4}$$

where V = lateral force at the top of the column.

By rearranging Eq. (4), the lateral force, V, can be expressed as

$$V=\frac{(2M-P\Delta)}{L}=\frac{2M}{L}-\frac{P\Delta}{L}=V_0-\frac{P\Delta}{L} \tag{5}$$

where V_0 = lateral force that would be obtained by ignoring the $P-\Delta$ effect.

Shown in Fig. 2, as a consequence of $P-\Delta$ effects seen in Eq. (5), V decreases relative to V_0, as the displacement, Δ, increases. This equation can also be expressed as

$$V=V_0-\frac{P\Delta}{L}=V_0-\theta K_0\Delta \tag{6}$$

where $\theta=P-\Delta$ stability factor given by

$$\theta=\frac{P}{K_0L} \tag{7}$$

From Eq. (6), the elastic stiffness considering $P-\Delta$, K_1 is therefore

$$K_1=K_0(1-\theta) \tag{8}$$

Similarly, the lateral force at which the column, including $P-\Delta$ effects, yields, V_{yp} is

$$V_{yp}=V_{y0}(1-\theta) \tag{9}$$

When elastic-perfectly plastic material properties are assumed for the idealized frame described earlier, lateral force V_0 in Eq. (6) remains constant in the postelastic region of the force-displacement graph as the plastic moment, M_p, is developed. However, when $P-\Delta$ effects are considered, the corresponding lateral force versus displacement curve exhibits a negative slope past the yield point, with stiffness of

$$K_2=-\theta K_0 \tag{10}$$

as shown in Fig. 2.

Therefore, the monotonic bilinear force-displacement response of a column in this SDOF structure, including $P-\Delta$ effects, can be summarized as follows:

$$V=\begin{cases}K_1\Delta & \text{if } \Delta\leqslant\Delta_y\\ V_{y0}+K_2\Delta & \text{if } \Delta>\Delta_y\end{cases} \tag{11}$$

The ultimate displacement of the structure is designated as Δ_u, as shown on Fig. 2, the point at which the postelastic lateral strength curve or negative slope intersects the displacement axis. This theoretically implies that, for any additional lateral displacement, lateral instability develops (i.e., the lateral strength becomes negative for any additional positive displacement).

Some additional parameters are useful to further characterize inelastic behavior of columns up to collapse. The ratio of postelastic to elastic stiffness, K_2 and K_1, respectively, known as the stiffness ratio, r, is given by

$$r=\frac{K_2}{K_1}=\frac{\alpha-\theta}{1-\theta} \tag{12}$$

where αK_0 = stiffness (in the absence of stability effects) of the strain-hardening segment of a bilinear elastic-plastic material model. Here, a value of $\alpha=0.0$ is considered throughout.

The displacement ductility, i.e., displacement as the ratio of yield displacement, at ultimate displacement, Δ_u, known as the static stability limit, μ_s, is derived from the geometry and relations given in Fig. 2, in terms of θ and r

$$\mu_s=\frac{\Delta_u}{\Delta_y}=1/\theta=1-1/r \tag{13}$$

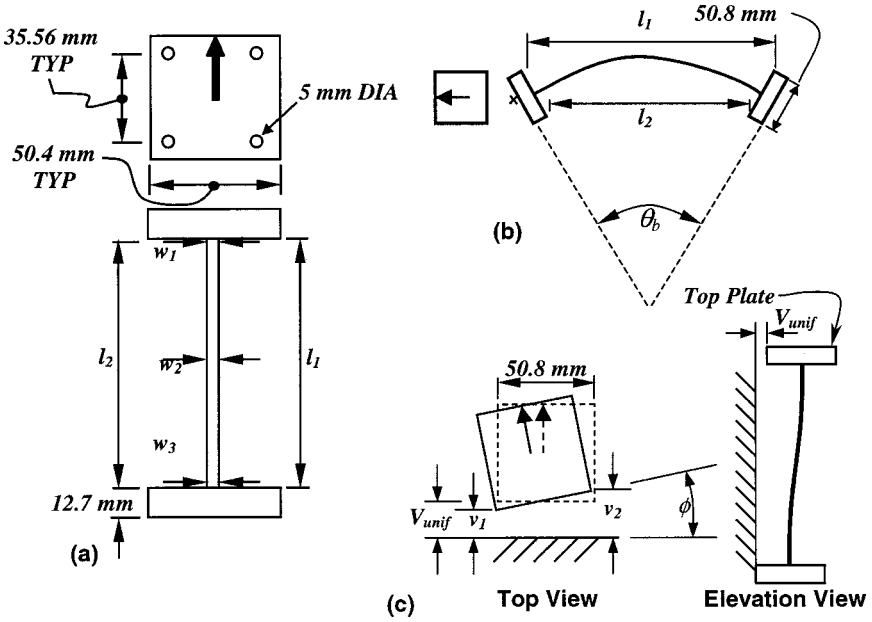

Fig. 3. (a) Specimen measurements in U–D orientation; (b) angle of bowing in U–D orientation; and (c) lateral shift in U–D orientation

Hysteresis Center Curve Concept

MacRae and Kawashima (1993) proposed the hysteresis center curve (HCC) concept to characterize the stability of general hysteresis loops. For the case of a bilinear system assumed for the analysis in this research, the HCC is a line parallel to the secondary stiffness that passes through the origin of the force-displacement space. If the secondary stiffness, K_2, is positive, the system is considered stable and after the structure yields will tend to return to the point of zero displacement upon repeated reverse cyclic yielding during ground shaking. However, if K_2 is negative, the structure is deemed to be dynamically unstable, and will tend to drift in a given direction once yielding has started. This results in large cumulative residual displacement and a lower cyclic energy absorption capacity. MacRae and Kawashima stated that, due to these large displacements, structures may be difficult to straighten and may perform poorly in a subsequent earthquake.

Amplification Factors for P–Δ Effects

Bernal (1987) investigated dynamic $P-\Delta$ effects in elastic and inelastic systems through the use of amplification factors. The ratio between displacement spectra with and without gravity effects represents the amplification spectrum that will amplify the elastic displacement for design.

Inelastic $P-\Delta$ analyses were performed using four ground motions for a series of time history analyses. Damping was held constant at 5% of critical while the target displacement ductility and stability factor were both varied, from 1 to 6 and from 0 to 0.2, respectively, providing a total of 192 amplification spectra.

In the course of Bernal's parametric study, the target ductility was made to satisfy a maximum limit $=0.4\mu_s$, based on the requirement that the structure must remain fit to resist the factored gravity load following the inelastic response. In addition, the derivation assumed that the postearthquake permanent deformation was equal to the maximum response ductility. Based on a statistical analysis of the 192 spectra generated in the study, the following expression for the amplification factor was proposed:

$$\alpha = \frac{1+\beta\theta}{1-\theta} \tag{14}$$

where regression analysis for the mean amplification yielded

$$\beta = 1.87(\mu - 1) \tag{15}$$

Overview of Experimental Program

Description of Specimens

A typical specimen column is shown in Fig. 3(a). The sizes of the specimens and masses of the 15 specimens tested are listed in Table 1 along with bilinear behavioral properties for the average dimensions, according to the SDOF model described previously. Specimens were designed to have slenderness ratios of 100, 150, and 200. A range of values for axial capacity versus demand, P_u/P_n, was chosen for each slenderness ratio, where P_u = weight of the mass plates used in the test, and P_n = axial capacity of all columns in the specimen, calculated using the AISC-LRFD specifications (AISC 1994). These values are listed, for each specimen, in Table 1.

Individual columns were cut from hot-rolled steel plate and then milled to size. A 50.8 mm (2 in.)-wide square by 12.7 mm (0.5 in.)-thick base plate was attached to the top and bottom of the column so that a rigid connection could be provided to both the shaking table and the mass plates above.

Thin metal strips were used as cross bracing to prevent out-of-plane movement and torsion of the test structures. The strips were sufficiently thin to add only negligible stiffness in the direction of shaking. This was verified analytically, as well as by free vibration tests which showed no change in the period of the structure with and without metal strip bracing. Free vibration tests showed no significant change in damping between the bare and braced specimen.

The 0.91 m×1.52 m (3 ft×5 ft) SDOF shaking table used for this testing program is driven by a displacement controlled 24.47

Table 1. General Properties and Fundamental Period Comparison of Specimens Tested

Specimen	Column height (mm)	Column width (mm)	Mass (kg/col)	P_u/P_n	K_0 (N/mm)	θ	K_1 (N/mm)	K_2 (N/mm)	T_{np} (s)	$T_{n\,\mathrm{exp}}$ (s)	ΔT_n (%)
					(a) $kL/r=100$						
1	137.2	4.8	36.63	0.09	40.27	0.065	37.65	−2.62	0.196	0.200	1.93
2	137.4	4.9	72.23	0.171	41.79	0.123	36.64	−5.16	0.279	0.272	−2.50
4	137.5	4.8	96.03	0.243	39.12	0.175	32.27	−6.85	0.343	0.323	−5.86
5b	91.7	2.9	96.03	0.814	23.60	0.435	13.33	−10.27	0.533	0.698	30.93
					(b) $kL/r=150$						
6	412.4	9.4	96.03	0.14	22.56	0.101	20.28	−2.28	0.432	0.430	−0.55
7	343.7	7.7	96.03	0.215	17.70	0.155	14.96	−2.74	0.503	0.490	−2.66
8	274.5	6.0	96.03	0.369	12.88	0.266	9.45	−3.43	0.634	0.655	3.39
9	205.8	4.8	96.03	0.54	11.75	0.390	7.17	−4.58	0.727	0.760	4.52
10	137.0	3.1	48.58	0.64	7.54	0.461	4.06	−3.48	0.687	0.662	−3.68
10b	137.4	2.8	48.58	0.943	6.88	0.504	3.41	−3.47	0.750	0.727	−3.01
					(c) $kL/r=200$						
11	549.5	9.4	72.23	0.191	9.34	0.138	8.05	−1.29	0.595	0.597	0.32
12	458.2	7.7	72.23	0.297	7.21	0.214	5.67	−1.55	0.709	0.682	−3.85
13	366.1	6.0	72.23	0.497	5.40	0.359	3.46	−1.93	0.908	0.959	5.61
14	275.2	4.7	72.23	0.738	4.84	0.532	2.26	−2.57	1.123	1.200	6.90
15	182.8	3.1	36.63	0.869	3.14	0.627	1.17	−1.97	1.111	1.004	−9.63

kN (5.5 kip) actuator. A displacement record generated from the ground acceleration time history for the El Centro Imperial Valley earthquake of May 1940, S00E component, was used in this study. Note that ground motion was not time scaled since the specimens were designed to fit actual parameters of interest, and not intended to be scaled models of actual structures.

Measurement of Initial Imperfections

Imperfections were thoroughly documented for each column in each specimen prior to testing. One base plate for each column of a specimen was marked with an arrow, establishing a reference orientation from which all measurements are related in each orthogonal direction, noted as ''U–D'' and ''L–R'' (for up–down and left–right). Fig. 3 schematically shows general column measurements and associated imperfections for the U–D orientation (similar data were also collected for the L–R direction). The width of each column was measured at the top, middle, and bottom, in each direction (w_1, w_2, and w_3, respectively). The free height between base plates, l_1 and l_2, was used to calculate the angle of bowing, θ_b. The top lateral shifts of the column, v_1 and v_2, were measured at each corner of the top base plate for each specimen column to allow calculation of the average uniform lateral shift, V_{unif}, and the angle of twist, ϕ. Note that, in assembling the specimens, column orientations were chosen so as to minimize the net sum of V_{unif} for all columns parallel and perpendicular to the direction of shaking. The dimensions measured and resulting imperfections are provided elsewhere (Vian and Bruneau 2001).

Instrumentation

A schematic of the test setup and instrumentation is shown in Fig. 4.

One accelerometer was mounted on the shaking table to measure the ground acceleration exerted on the model structure. Two were mounted on top of the specimen, on the east and west sides of the mass plates, to measure the total acceleration of the mass, from which the inertial force acting on it can be calculated.

A strain gauge was mounted on one column of each specimen, and located a distance of one-third of the column height from its bottom base plate. This gauge was used to estimate structural forces during shake table testing, and subsequently during tests to establish material properties. Temposonics magnetostrictive displacement transducers were used to measure displacement of the table (labeled UG), vertical displacement of the mass (labeled Vert), and total horizontal (and torsional if any) displacements at the east and west sides of the mass (labeled HorEast and HorWest, respectively).

Measurement of displacements of the structural mass during the entire structural response of the specimens, including throughout much of their collapse, required special modifications to the instrument setup, described elsewhere (Vian and Bruneau 2001).

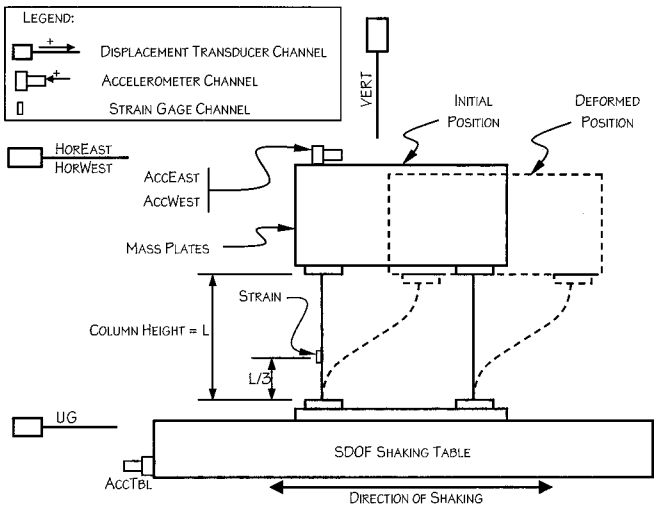

Fig. 4. Schematic of test setup and instrumentation (looking west)

Testing of Specimens

Results from the linear elastic free vibration test first performed on each specimen before subjecting it to earthquake excitations were used to determine the fundamental period of vibration and damping properties of the specimens. Table 1 lists, using average dimensions for each column making up the structure, the predicted fundamental period of vibration including $P-\Delta$ effects, T_{np}, the period calculated from the experimentally obtained time history data using Fourier spectrum analysis, $T_{n\,\mathrm{exp}}$, and the percent of difference between the two values, ΔT_n.

The percentage of critical damping due to inherent damping in the structure, ξ, was also estimated from the free vibration time history data using a logarithmic decrement method (Clough and Penzien 1993). The free vibration response curve obtained for each specimen was divided into three approximately equal intervals and estimates of the damping ratio were made using the first and last peaks of each interval. Interestingly, the resulting damping was found to be highly nonlinear. In general, when the mean amplitude of vibration of a given interval is plotted versus the estimated damping ratio for that interval, an inverse relationship between the two variables was observed (Vian and Bruneau 2001).

Shake table test schedules were established for each specimen, thus creating a series of progressively more severe shake table tests until the structure collapsed. The peak ground acceleration (PGA), for which maximum specimen displacement is equal to yield, was estimated using the 1.5% damped elastic response spectrum. Similarly, the PGA for collapse of a SDOF bilinear model was estimated, using the inelastic spectrum technique, and time history analyses by calculating the minimum value at which the displacement of the system is equal to the ultimate displacement, Δ_u. From this information, approximately five PGA values were chosen to subject each of the specimens to during testing, progressively and proportionally increasing values in magnitude from approximately two-thirds of the estimated peak elastic response to the estimated peak inelastic response.

Experimental Results and Observations

Peak response quantities for the entire series of tests to which all specimens were subjected are normalized and plotted to investigate whether behavioral trends exist as a function of some of the key parameters defined previously. The progressive test results are then compared to empirical limits proposed by others to minimize $P-\Delta$ effects on highway bridge piers, as well as to prediction of ''survivability'' inferred from axial-moment strength interaction design equations that consider both first- and second-order effects.

Behavioral Trends

The value of the stability factor, θ, has a significant effect on the response of the structure. In practical bridge and building structures, θ is unlikely to be greater than 0.10, and is generally less than 0.060 (MacRae et al. 1993). Specimen 1 is found to be the only one here that has a θ value near the suggested practical range for the stability factor, that is, with a value of 0.065. Specimens 2, 6, and 11 have stability factors slightly larger than the likely upper limit, at 0.123, 0.101, and 0.138, respectively. All other specimens have a value of $\theta \geqslant 0.155$.

Results of a graphical study of peak response parameters are summarized below. The spectral acceleration for the observed specimen period, $S_{a\,\mathrm{final}}$, displacement ductility, μ_{final}, and drift, γ_{final}, of the penultimate shake table test were compared with the stability factor, θ, and the static stability limit, μ_s, of each specimen. Each of these values is from the penultimate test in a schedule of increasing earthquake intensity tests. Residual displacements of varying degrees are observed at the conclusion of each test as the schedule progresses. The following general observations can be made:

- The elastic spectral acceleration for the observed specimen period, S_a, the peak displacement ductility, μ, and peak percent of drift as a percentage of the height, γ, were observed for the penultimate shake table test to have inverse relationships with θ. This suggests that the structures may be less able to undergo large inelastic excursions before imminent instability as the stability factor increases. Specimens 1 and 6, which have the lowest values of θ tested, were the only specimens able to withstand ground motion that imparted elastic spectral acceleration greater than 0.75 g.
- Specimen 1 was the only specimen that underwent both ductility greater than five (20.35) and drift larger than 20% of the specimen height (64%), prior to collapse. Recall that this is the only specimen that has a value of θ less than 0.1.

The static stability limit, μ_s, can be expressed as the inverse of the stability factor, as previously demonstrated. A reverse trend of that seen versus the stability factor is observed, as expected, when the same response parameters are compared to μ_s. In Fig. 5, peak displacement ductility for the penultimate test is plotted versus the static stability limit (a best-fit equation has been matched to the data). The line $\mu_{\mathrm{final}} = \mu_s$ is shown for clarity. Only specimen 1 was able to achieve ductility greater than the static stability limit in the next to last test.

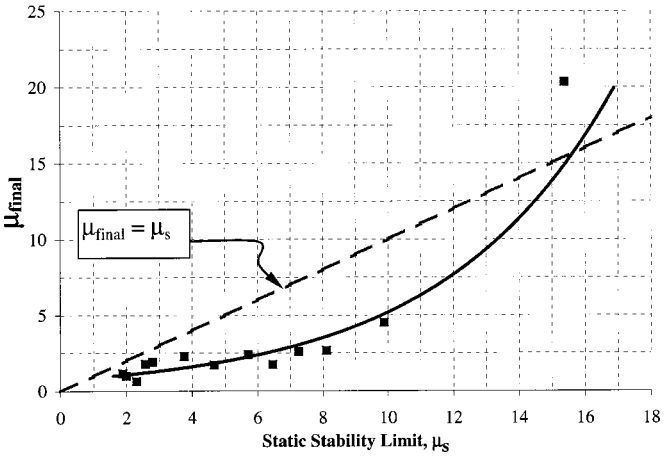

Fig. 5. Peak displacement ductility-penultimate test versus stability factor

NCHRP 12-49 Proposed P–Δ Limits for Bridge Piers

The National Cooperative Highway Research Program (NCHRP), Project 12-49, under the auspices of the Transportation Research Board, developed a comprehensive set of proposed revisions to the American Association of State Highway Transportation Organizations (AASHTO) LRFD seismic specifications for highway bridges (ATC/MCEER 2001). Included is a proposed provision, intended to limit $P-\Delta$ effects on bridge piers, which states the following:

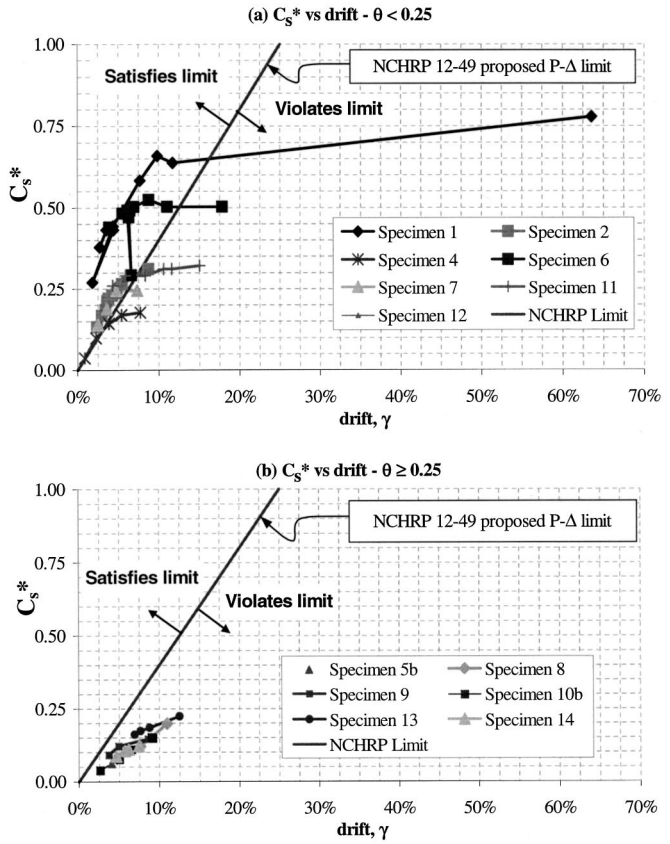

Fig. 6. Comparison of test results with NCHRP 12-49 limits

The displacement of a pier or bent in the longitudinal and transverse direction must satisfy

$$\Delta_m \leqslant 0.25C\left(\frac{W}{P}\right)H \tag{16}$$

where $\Delta_m = R_d\Delta$; R_d = factor related to a response modification factor and fundamental period; Δ = displacement demand from seismic analysis; C = seismic base shear coefficient based on lateral strength; W = weight of the mass participating in the response of the pier; P = vertical load on the pier from nonseismic loads; and H = height of the pier.

For analysis of the specimens in this research, $W = P$ and the measured experimental displacements, u_{rel}, and estimated base shear coefficient, C_s^* $(= V_p^*/W)$, can substitute for Δ_m and C, respectively, in Eq. (16). Note that V_p^* is the experimentally estimated base shear, corrected for $P-\Delta$, described elsewhere (Vian and Bruneau 2001).

In Fig. 6 the proposed limit is compared with the peak experimental responses. The estimated base shear coefficient, C_s^*, is plotted as a function of the maximum drift, γ $(= u_{\text{rel}}/H)$. In Fig. 6(a), the specimens for which $\theta < 0.25$ (1, 2, 4, 6, 7, 11, and 12) are shown. During the initial tests, when the proposed limit was satisfied, none of these specimens failed. However, in the subsequent tests, due to repeated inelastic action, cumulative drifting of the structure increased, eventually causing progressive collapse and violation of the proposed limit. Collapse always occurred only after the limit was exceeded in a prior test, thus validating the proposed criterion. As shown in Fig. 6(b), the remaining specimens, for which $\theta \geqslant 0.25$, never satisfied the drift criteria, even for those tests that remained in the elastic range. The stability factor for these specimens, however, is well above the practical range discussed previously and, therefore, the limit violation is of no consequence.

Specimen Stability Analysis

The shake table test data are compared with axial-moment interaction design equations that account for both first-order and second-order behavior. The following bilinear relation is used to represent first-order strength of the specimen, accounting for first-order column stability, by AISC (1994):

$$\frac{8}{9}\frac{M_{pr}}{M_p} + \frac{P_u}{P_n} = 1 \quad \text{for } \frac{P_u}{P_n} \geqslant 0.2$$
$$\frac{M_{pr}}{M_p} + \frac{P_u}{2P_n} = 1 \quad \text{for } \frac{P_u}{P_n} < 0.2 \tag{17}$$

where M_p = plastic moment capacity of the section; M_{pr} = reduced plastic moment capacity due to the presence of an axial load; P_u = axial load on the column; and P_n = axial compressive strength of the column.

Note that this equation, as shown, does not address additional moment demand due to $P-\Delta$ effects. Second-order moment magnification due to $P-\Delta$ effects can be accounted for by the use of the AISC-LRFD factor, B_2. This factor amplifies static load effects, and, for the case under consideration, can be simplified as follows:

$$B_2 = \frac{1}{1 - \dfrac{\Sigma P_u \Delta}{\Sigma VL}} = \frac{1}{1 - \dfrac{P_u}{KL}} = \frac{1}{1-\theta} \tag{18}$$

The above interaction relation of Eq. (17) can be used to calculate the minimum spectral acceleration necessary for structural instability of the specimens. Solving for the reduced moment capacity at the given constant axial force present on the structure, M_{pr}, the limiting base shear, V_{lim}, that corresponds to this moment can be calculated as

$$V_{\text{lim}} = \frac{2M_{pr}}{L} \tag{19}$$

The corresponding elastic spectral acceleration is

$$S_{a\,\text{lim}} = \frac{RV_{\text{lim}}}{W} \tag{20}$$

Second-order effects can be accounted for during the elastic range of behavior by dividing the right side of Eq. (20) by B_2, further reducing the moment capacity, M_{pr}, in Eq. (19). This also leads to a reduction in the limiting base shear and corresponding spectral acceleration that the structure can withstand, as shown above.

Inelastic systems must be analyzed in a slightly different manner. Typically, assuming equivalent inelastic and elastic maximum displacement (Newmark and Hall 1982), the design shear force will be reduced by the ratio of elastic to inelastic response force, designated the response modification factor, R. The resulting modification of Eq. (18) is

$$B_2 = \frac{1}{1 - R\theta} \tag{21}$$

Note that, for $R = 4$, typically considered for an ordinary moment frame, as the stability factor approaches 0.25, the denominator of the expression approaches 0, and therefore, B_2 approaches infinity. When $\theta > 0.25$, this moment magnification

Table 2. First-Order Strength and Stability Analysis

Specimen	Weight (N)	Column height (mm)	P_u/P_n	M_p (N·mm)	AISC interaction [AISC 1994, Eq. (17)] M_{pr} (N·mm)	M_p (%)	V_{lim} (N)	$S_{a\,\text{lim}}$ (g)
				(a) $kL/r=100$				
1	359.2	137.2	0.09	11,835	11,301	95.5	164.7	0.459
2	708.3	137.4	0.171	12,791	11,697	91.4	170.3	0.240
4	941.8	137.5	0.243	11,911	10,148	85.2	147.6	0.157
5b	941.8	91.7	0.814	6,070	1,268	20.9	27.7	0.029
				(b) $kL/r=150$				
6	941.8	412.4	0.14	75,735	70,420	93.0	341.5	0.363
7	941.8	343.7	0.215	43,820	38,718	88.4	225.3	0.239
8	941.8	274.5	0.369	23,153	16,424	70.9	119.7	0.127
9	941.8	205.8	0.54	11,879	6,146	51.7	59.7	0.063
10	476.4	137	0.64	2,265	919	40.6	13.4	0.028
10b	476.4	137.4	0.943	5,904	378	6.4	5.5	0.012
				(c) $kL/r=200$				
11	708.3	549.5	0.191	81,279	73,505	90.4	267.5	0.378
12	708.3	458.2	0.297	33,414	26,421	79.1	115.3	0.163
13	708.3	366.1	0.497	23,531	13,313	56.6	72.7	0.103
14	708.3	275.2	0.738	11,675	3,445	29.5	25.0	0.035
15	359.2	182.8	0.869	2,166	320	14.8	3.5	0.010

factor is negative. Note that the inelastic amplification factor, α, presented previously (Bernal 1987), is conceptually similar to in Eq. (21), but does not suffer from this mathematical singularity.

The resulting elastic spectral acceleration capacity is calculated by removing the response modification factor from the equation (i.e., $R=1$). From the perspective of comparison with interaction relations, this is equivalent to the spectral acceleration producing first yield by assessing elastic behavior up to M_{pr}. These quantities are listed for the specimens tested in Tables 2 and 3 for first-order and second-order analyses, respectively.

Table 4 compares the maximum and minimum calculated spectral acceleration with the maximum measured mass acceleration, $\ddot{u}_{T\,\max}$, and the maximum estimated base shear coefficient, C_{so}^* and C_s^*, respectively, calculated by neglecting and including $P-\Delta$ effects. Each of the specimens reached values of these factors that exceed the minimum calculated spectral acceleration, which was dictated by the inelastic moment amplification factor, α.

The maximum calculated spectral acceleration was dictated by the section strength limit equation in all instances. Only specimen

Table 3. Second-Order Strength and Stability Analysis

Specimen	M_p (N·mm)	θ	Amplification factors α ($\mu=4$)	B_2 ($R=4$)	α or B_2 ($\mu=R=1$)	α ($\mu=R=4$) M_{pr} (N·mm)	M_p (%)	V_{lim} (N)	$S_{a\,\text{lim}}$ (g)	B_2 ($R=4$) M_{pr} (N·mm)	M_p (%)	V_{lim} (N)	$S_{a\,\text{lim}}$
					(a) $kL/r=100$								
1	11,835	0.065	1.46	1.35	1.07	7,742	65.4	89.6	0.249	10,566	89.3	144.6	0.403
2	12,791	0.123	1.93	1.97	1.14	6,060	47.4	59.1	0.083	10,254	80.2	132.9	0.188
4	11,911	0.175	2.4	3.34	1.21	4,224	35.5	36.1	0.038	8,372	70.3	103.6	0.110
5b	6,070	0.435	6.09	−1.35	1.77	208	3.4	1.7	0.002	716	11.8	10.9	0.012
					(b) $kL/r=150$								
6	75,735	0.101	1.74	1.68	1.11	40,368	53.3	139.4	0.148	63,292	83.6	278.8	0.296
7	43,820	0.155	2.21	2.63	1.18	17,514	40.0	62.9	0.067	32,724	74.7	164.9	0.175
8	23,153	0.266	3.4	−15.17	1.36	4,829	20.9	17.0	0.018	12,048	52.0	69.3	0.074
9	11,879	0.39	5.22	−1.79	1.64	1,178	9.9	4.5	0.005	3,752	31.6	26.2	0.028
10	2,265	0.461	6.66	−1.18	1.86	138	6.1	0.7	0.001	495	21.8	4.9	0.010
10b	5,904	0.504	7.72	−0.98	2.02	49	0.8	0.2	0.000	188	3.2	1.8	0.004
					(c) $kL/r=200$								
11	81,279	0.138	2.06	2.23	1.16	35,714	43.9	83.8	0.118	63,362	78.0	202.7	0.286
12	33,414	0.214	2.8	7.01	1.27	9,426	28.2	22.2	0.031	20,759	62.1	74.6	0.105
13	23,531	0.359	4.69	−2.3	1.56	2,836	12.1	6.4	0.009	8,540	36.3	34.3	0.048
14	11,675	0.532	8.52	−0.89	2.14	404	3.5	0.9	0.001	1,612	13.8	7.6	0.011
15	2,166	0.627	12.09	−0.66	2.68	26	1.2	0.1	0.000	120	5.5	0.8	0.002

Table 4. Comparison of Measured Acceleration and Base Shear Coefficients with Analytical Values

Specimen	$S_{a\,\min}$[a] (g)	$S_{a\,\max}$[b] (g)	$\ddot{u}_{T\,\max}$ (g)	$\frac{\ddot{u}_{T\,\max}-S_{a\,\min}}{S_{a\,\min}}$ (%)	$\frac{\ddot{u}_{T\,\max}-S_{a\,\max}}{S_{a\,\max}}$ (%)	C^*_{so} (g)	$\frac{C^*_{so}-S_{a\,\min}}{S_{a\,\min}}$ (%)	$\frac{C^*_{so}-S_{a\,\max}}{S_{a\,\max}}$ (%)	C^*_s (g)	$\frac{C^*_s-S_{a\,\min}}{S_{a\,\min}}$ (%)	$\frac{C^*_s-S_{a\,\max}}{S_{a\,\max}}$ (%)
					(a) $kL/r=100$						
1	0.249	0.459	0.607	143.4	32.4	0.778	212.0	69.6	0.561	125.0	22.3
2	0.083	0.240	0.253	203.4	5.2	0.312	274.1	29.8	0.226	170.5	−6.2
4	0.038	0.157	0.173	351.0	10.4	0.177	361.4	12.9	0.115	199.4	−26.7
5b	0.002	0.029	0.017	866.8	−42.1	0.061	3,369.1	107.7	0.021	1,068.0	−30.1
					(b) $kL/r=150$						
6	0.148	0.363	0.381	157.5	5.1	0.524	254.1	44.5	0.436	194.7	20.3
7	0.067	0.239	0.222	232.2	−7.2	0.245	266.6	2.4	0.198	196.5	−17.2
8	0.018	0.127	0.110	508.2	−13.4	0.199	1,000.3	56.6	0.090	396.4	−29.4
9	0.005	0.063	0.058	1,121.0	−8.5	0.147	2,994.6	131.8	0.073	1,442.8	15.6
10	0.001	0.028	—	—	—	—	—	—	—	—	—
10b	0.000	0.012	0.052	10,382.5	350.2	0.153	30,742.8	1,224.6	0.063	12,596.5	445.3
					(c) $kL/r=200$						
11	0.118	0.378	0.352	197.7	−6.8	0.322	172.3	−14.7	0.233	96.7	−38.4
12	0.031	0.163	0.184	488.3	13.0	0.300	859.3	84.3	0.225	619.7	38.2
13	0.009	0.103	0.103	1,046.3	0.3	0.224	2,393.0	118.1	0.099	996.5	−4.1
14	0.001	0.035	0.035	2,539.0	−1.0	0.121	9,023.3	242.4	0.048	3,542.1	36.7
15	0.000	0.010	—	—	—	—	—	—	—	—	—

[a]Minimum value of spectral acceleration, $S_{a\,\lim}$, from Tables 2 and 3.

[b]Maximum value of spectral acceleration, $S_{a\,\lim}$, from Tables 2 and 3.

1, the only one with $\theta<0.1$, reached a value of $\ddot{u}_{T\,\max}$ that exceeded its corresponding $S_{a\,\max}$. Considering the base shear coefficient without $P-\Delta$ effects, C^*_{so}, all of the specimens for which this value exceeds $S_{a\,\max}$ have $\theta<0.4$, although not all specimens in this range of stability factor reached this state. Specimens 1, 6, and 12 all reached values of the base shear coefficient with $P-\Delta$ effects, C^*_s, larger than that of the maximum calculated spectral acceleration.

Model Verification Example

Analytically and experimentally obtained lateral force versus displacement results were compared for specimen 11 for its entire series of tests by performing nonlinear dynamic analyses using a bilinear elastically perfect plastic model. An average damping ratio estimate of 1.80% was used for each analysis. The bilinear parameters of the virgin specimen specified in the NONLIN (Charney 1998) model were obtained from data previously presented and described above. Yield stress observed during tension testing was used to determine the plastic base shear (including $P-\Delta$), V_{yp}, and the yield displacement, $\Delta_y=255$ N, and 31.67 mm, respectively. However, when the specimen experienced residual displacement at the conclusion of a test, the model was modified for the subsequent test to account for the lower yield base shear upon reloading due to $P-\Delta$ effects and bias in the cumulative drifting.

Note that the specimens tested exhibit the dynamically unstable behavior characteristic of negative postyield stiffness, and negative HCC, as described previously. As a result, the system has a tendency to drift in a given direction once yielding has started, resulting in large cumulative residual displacement and a lower cyclic energy absorption capability prior to failure.

Fig. 2 shows, for the assumed bilinear force-displacement model, the reduced specimen yield level, V'_{yp}, following residual displacement, u_r, given by

$$V'_{yp}=V_{yp}-\Delta F_y=K_1(\Delta_y-\theta u_r) \tag{22}$$

where ΔF_y=specimen yield base shear reduction, and all other terms have been defined.

Two series of bilinear dynamic analyses were performed: First, the experimentally obtained residual displacement from each test was used to calculate the reduced yield force for the subsequent analysis (referred to as method 1 hereafter). Second, the residual displacement obtained analytically was used to calculate the re-

Table 5. Yield Force Reductions, Specimen 11

	Method 1			Method 2		
Test	V'_{yp} (N)	u_r (mm)	ΔF_y (N)	V'_{yp} (N)	u_r (mm)	ΔF_y (N)
1	255.0	0.7	−0.8	255.0	0.0	0.0
2	254.2	3.1	−3.4	255.0	0.0	0.0
3	251.6	12.8	−14.2	255.0	17.0	−18.9
4	240.8	24.3	−27.0	236.1	60.7	−67.4
5	228.0	35.7	−39.7	187.6	91.5	−101.6
6	215.3	63.2	−70.2	153.4	∞	–
7	184.8	—	—	—	—	—

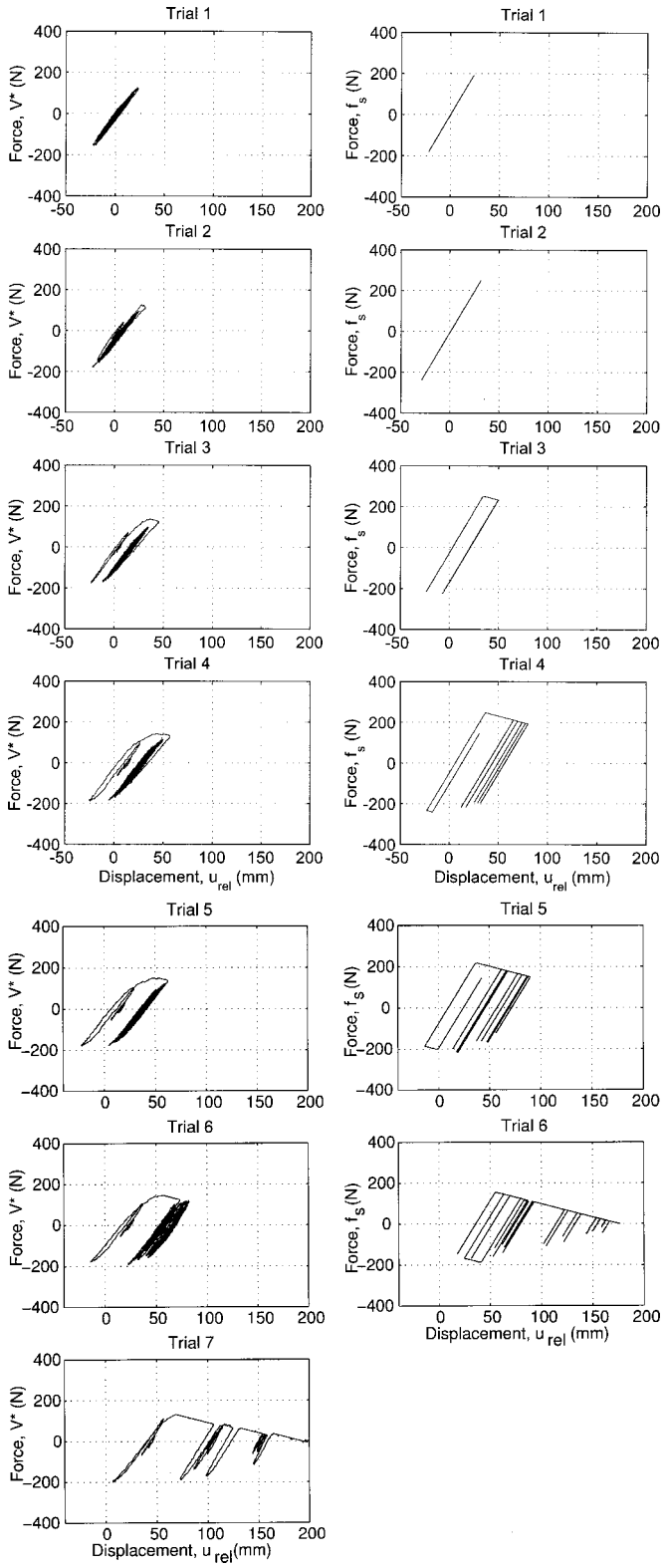

Fig. 7. Force displacement; specimen 11, expt versus method 1

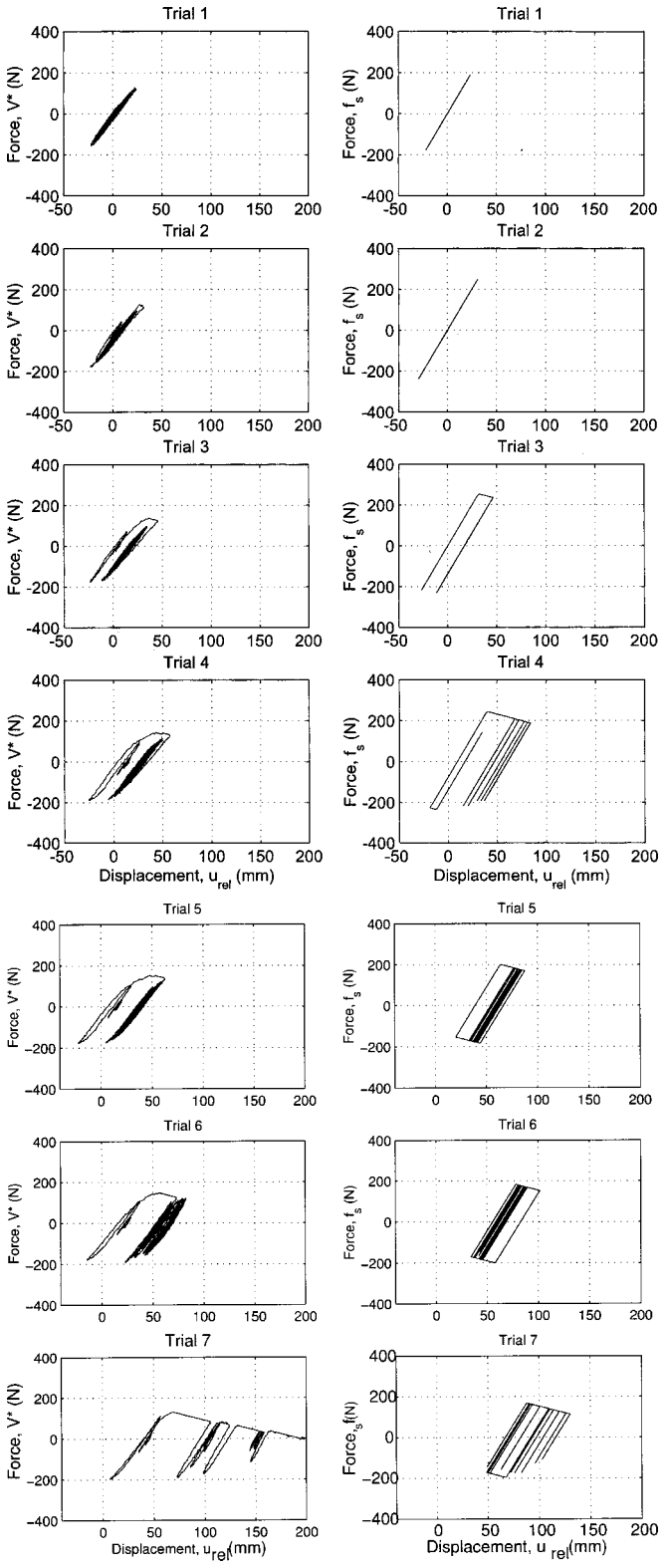

Fig. 8. Force displacement; specimen 11, expt versus method 2

duced yield force (method 2). Note that method 2 is a purely analytical approach, whereas method 1 is a hybrid in that the experimental results are used to ''adjust'' each successive analysis.

Table 5 summarizes the residual displacement and reduced yield force values obtained using each of these methods. Analytical results are plotted next to the experimental results for each of the two methods in Figs. 7 and 8, respectively. The experimental results are displayed in the left column of Figs. 7 and 8 using the experimentally estimated base shear corrected for $P-\Delta$, V_p^*, and relative horizontal displacement [corrected as described and reported earlier (Vian and Bruneau 2001)]. The analytical results are in the right column of Figs. 7 and 8 and display the analytical base shear force, f_s, versus the relative displacement. Note that

neither method provides a good match with experimental data, and that the second method predicted collapse before the final test.

Note that these analyses are used for illustration purposes only. It is expected that more accurate refined analytical models will be used, calibrated, and developed to match, until collapse, the data from these benchmark experiments. Some work in this direction has already been conducted (Sivaselvan and Reinhorn 2002).

Conclusion

Fifteen SDOF specimens were subjected to earthquakes of progressively increasing intensity up to collapse due to instability. The purpose of the tests was to produce a set of fully documented benchmarks to which analytical models could be compared. In addition, a number of observations were made from the collected experimental data for consideration in the design of slender steel structures that behave inelastically under seismic excitation.

This study applies to structures that generally exhibit bilinear behavior. It is therefore felt that the results could be applicable to both steel and concrete structures, if details of proper practices are employed in order to ensure the reliable ductile performance desired during an earthquake event. Future studies could investigate structures that exhibit other hysteresis types.

The stability factor, θ, was observed to have the most significant effect on the structure's propensity to collapse. As θ increases, the maximum attainable ductility, sustainable drift, and spectral acceleration, which can be reached before collapse, all decrease. When this factor was larger than 0.1, the ultimate values of maximum spectral acceleration, displacement ductility, and drift reached before collapse were all grouped below values of 0.75 g, 5, and 20%, respectively.

Data collected in this test program were also used to verify the adequacy of an equation proposed to limit $P-\Delta$ effects in highway bridges. Collapse always occurred only after the limit prescribed by that equation was exceeded in a prior test, thus validating the proposed criterion.

In a comparison of experimental results versus the capacities predicted by design interaction equations, all specimens were observed to have exceeded the strength predicted by inelastic moment amplification factors. In addition, some specimens having a low stability factor actually exceeded the strength calculated based on first-order effects. Considering the measured base shear coefficient without $P-\Delta$ effects, C_{so}^{*}, all of the specimens for which this value exceeds $S_{a\,\max}$ have a stability factor of less than 0.4, although not all specimens in this range reached this state.

For similar test programs in the future, specimens could be tested under other conditions to further quantify the nonlinear inelastic behavior of columns under earthquake loads up to collapse. For example, ground motion, measured or synthesized, with a more uniform response spectrum over the entire frequency range under consideration may be more desirable in removing the impact of ground motion as a variable that affects the behavior of the specimens. Alternatively, the effects of large pulses (near-fault effects) versus more regular cyclical excitations could be considered. It would also be of particular importance to more accurately quantify the effect of the stability factor, especially in the range of most practical significance, in relation to various peak response parameters, including those investigated in this study.

Acknowledgments

This work was supported in part by the Earthquake Engineering Research Centers Program of the National Science Foundation under Award No. ECC-9701471 to the Multidisciplinary Center for Earthquake Engineering Research. However, any opinions, findings, conclusions, and recommendations presented in this paper are those of the authors and do not necessarily reflect the views of the sponsors.

References

American Institute of Steel Construction (AISC). (1994). *Manual of steel construction, load and resistance factor design*, 2nd Ed., AISC, Chicago, Ill.

ATC/MCEER Joint Venture. (2001). ''Recommended LRFD guidelines for the seismic design of highway bridges, Parts I and II, preliminary report.'' Based on NCHRP Project 12–49, *Rep. Nos. ATC-49a* (draft) and *MCEER 02-SP01*, November 2001, in press.

Bernal, D. (1987). ''Amplification factors for inelastic dynamic *p*-delta effects in earthquake analysis.'' *Earthquake Eng. Struct. Dyn.*, 15(5).

Charney, F. A. (1998). ''NONLIN: Nonlinear dynamic time history analysis of single degree of freedom systems.'' Federal Emergency Management Agency.

Clough, R. W., and Penzien, J. (1993). *Dynamics of structures*, 2nd Ed., McGraw–Hill, New York.

MacRae, G. A., and Kawashima, K. (1993). ''The seismic response of bilinear oscillators using Japanese earthquake records.'' *Journal of Research*, 30, Public Works Research Inst., Tsukuba, Japan.

MacRae, G. A., Priestley, M. J. N., and Tao, J. (1993). ''*P*-Δ effects in seismic design.'' *Rep. No. SSRP-93/05*, Dept. of Applied Mechanics and Engineering Sciences, Univ. of California, San Diego, Calif.

Newmark, N. M., and Hall, W. J. (1982), ''Earthquake spectra and design.'' *Original Monograph Series No. MNO–3*, Earthquake Engineering Research Institute, Berkeley, Calif.

Sivaselvan, M. V., and Reinhorn, A. M. (2002). ''Collapse analysis: Large inelastic deformation analysis of planar frames.'' *J. Struct. Eng.*, 128(12), 1575–1583.

Vian, D., and Bruneau, M. (2001). ''Experimental investigation of *p*-delta effects to collapse during earthquakes.'' *Technical Rep. No. MCEER 01-0001*, Multidisciplinary Center For Earthquake Engineering Research, Univ. at Buffalo, Buffalo, N.Y.; http://civil.eng.buffalo.edu/users_ntwk/experimental/case_studies/vian/.